Synthetic Metals 162 (2012) 2337–2341

Contents lists available at SciVerse ScienceDirect

Synthetic Metals

journal homepage: www.elsevier.com/locate/synmet

3D hierarchical porous carbons containing numerous nitrogen atoms as catalyst supports for PEMFCs

Young Soo Yun [a], Doyoung Kim [b], Hyun Ho Park [a], Yongsug Tak [b], Hyoung-Joon Jin [a,*]

[a] Department of Polymer Science and Engineering, Inha University, Incheon 402-751, Republic of Korea
[b] Department of Chemical Engineering, Inha University, Incheon 402-751, Republic of Korea

ARTICLE INFO

Article history:
Received 25 September 2012
Received in revised form 1 November 2012
Accepted 7 November 2012
Available online 20 December 2012

Keywords:
Catalyst support
Fuel cell
Nitrogen-doped carbon
Hierarchical
Porous materials

ABSTRACT

Hierarchical porous carbons containing numerous nitrogen atoms (HPCs-N) with high surface areas and 3D interconnected open macropore structures were prepared as a catalyst support for PEMFCs. Despite the large amount of Pt nanoparticles (40 wt%) highly dispersed Pt catalysts with homogeneous small diameters (~2 nm) were achieved using the effects of nitrogen sites. The electrochemical performances of a Pt-incorporated HPCs-N cathode were better than those of the Pt-incorporated carbon black cathode due to the improved carbon-catalyst binding, extension of the three-phase boundary, improved mass transfer, and a synergistic support effect with the nitrogen-doped support materials.

1. Introduction

Proton exchange membrane fuel cells (PEMFCs) have been of great interest as future energy sources for applications such as low/zero emission electric vehicles, distributed home power generators, and power sources for small portable electronics due to their high power density, relatively quick start up, rapid response to varying loads, and relatively low operating temperature [1,2]. However, wide application of PEMFC technology has been hindered by the high cost of the Pt catalyst and poor kinetics of the oxygen reduction reaction (ORR).

One of the main research targets in PEMFC technology is reducing the amount of electro-catalyst used in the cell without sacrificing its performance. Therefore, the efficient utilization of Pt catalysts is important in the practical applications of PEMFCs. Catalyst support technology has been proven as an effective approach to reduce the use of Pt catalysts and improve catalytic activity. The catalytic activity of Pt-based catalysts is strongly dependent on the catalyst support, which is very important in determining the size, degree of dispersion, distribution, and stabilization of the catalysts, as well as the catalytic surface area for the ORR [3]. In addition, efficient mass transfer of reactants can be achieved using catalyst supports with porous structure [4–13]. Particularly, the use of ordered mesoporous and macroporous carbon has induced superior catalytic effects [4–6]. Yu et al. reported an ordered uniform porous carbon network prepared by Al-implanted silica particles, which outperformed the commercial carbon black, E-TEK, by about 30–40% [6]. Fang et al. reported an ordered hierarchical nanostructured carbon prepared using a polystyrene sphere template, which exhibited greatly enhanced catalytic activity toward oxygen reduction reaction that was improved by about 53–88% compared to carbon black Vulcan XC-72. Recently, nitrogen-doped carbon materials have received considerable attention due to the strong electron donor nature of nitrogen, which can promote the enhancement of π bonding, leading to improved stability, electron transfer rate, and durability of the carbon supports during the electrocatalytic processes [14–16]. Imran Jafri et al. reported that nitrogen-doped multi-walled carbon nanocoils and graphene nanoplatelets used as catalyst supports led to improved maximum power densities compared with those of multi-walled carbon nanocoils and graphene nanoplatelets [17,18]. Chen et al. and Tuaev et al. reported that nitrogen-doped carbon nanotubes enhanced the electrocatalytic activity and stability of supported Pt nanoparticles [19,20].

In this study, 3D hierarchical porous carbons containing numerous nitrogen atoms (HPCs-N) were prepared from the inclusion complexes of cellulose hosted by urea hydrates [21]. The novel carbons had open macroporous structure, which is advantageous in the mass transfer of reactants, as well as high surface area and numerous nitrogen atoms. Pt nanoparticles were incorporated by a microwave-assisted ethylene glycol method. The 40 wt% Pt-incorporated HPCs-N (Pt-HPCs-N) were prepared as catalyst

* Corresponding author. Tel.: +82 32 860 7483; fax: +82 32 865 5178.
E-mail address: hjjin@inha.ac.kr (H.-J. Jin).

0379-6779/$ – see front matter © 2012 Elsevier B.V. All rights reserved.
http://dx.doi.org/10.1016/j.synthmet.2012.11.005

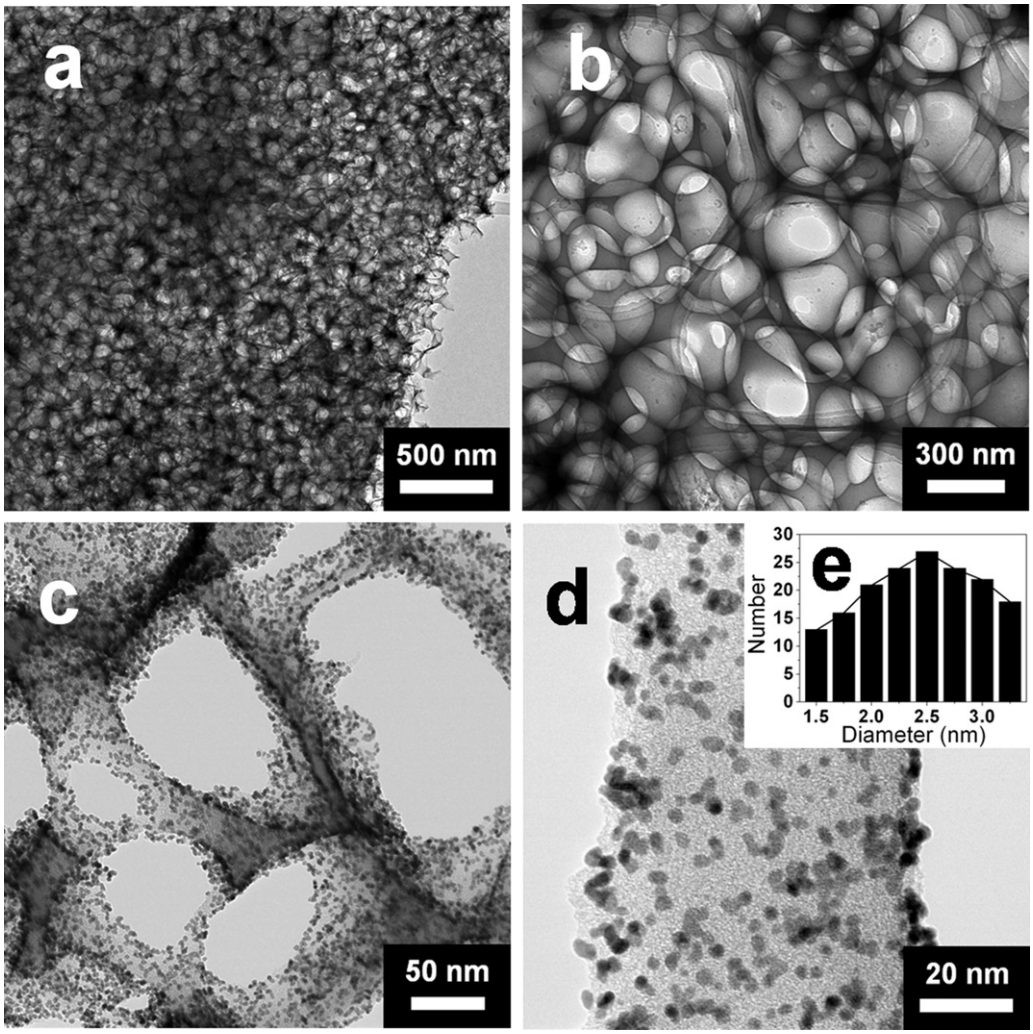

Fig. 1. TEM images of (a), (b) HPCs-N with different magnifications, and (c), (d) Pt-HPCs-N with different magnifications and (e) A size histogram of Pt nanoparticles estimated from (d).

supports for PEMFCs, and their electrochemical performances were compared with those of 40 wt% Pt-incorporated carbon black.

2. Experimental

2.1. Pt-HPCs-N fabrication

HPCs-N were prepared using a previously reported procedure [21]. A mixture of 7 wt% NaOH/12 wt% urea/81 wt% water solution pre-cooled to −12 °C for 2 h was prepared, and 4 wt% cotton cellulose (Aldrich) was immersed in the mixture solution, which was then intensely stirred for approximately 5 min at ambient temperature (IC solution). The IC solutions were then frozen at −196 °C and then freeze-dried for 3 days. The IC cryogel was carbonized from room temperature to 800 °C for 3 h. A heating rate of 5 °C/min and an Ar flow of 200 mL/min were applied. After the cryogel was carbonized, it was washed using distilled water and ethanol and then dried in a vacuum oven at 30 °C.

The Pt nanoparticles were incorporated into the HPCs-N using a microwave-assisted ethylene glycol method [7]. In particular, 5.0 mL of an aqueous solution of 0.05 M $H_2PtCl_6{\cdot}6H_2O$ was mixed with 150 mL of ethylene glycol in a 250-mL beaker. A total of 1.75 mL of 0.4 M KOH was then added dropwise to a vigorously stirred solution in order to adjust the pH to approximately 8–9. The required amount of HPCs-N was added to the mixture and ultrasonicated for 30 min. The beaker containing the mixture of Pt salts and HPCs-N was heated in a household microwave oven (Samsung RE-C20DV, 2450 MHz, 700 W) for 100 s. The resulting suspension was stirred vigorously overnight and filtered. The residue was washed thoroughly with deionized water and dried overnight at 80 °C.

2.2. Preparation of the Pt-HPCs-N cathode and membrane electrode assembly (MEA)

The fabricated Pt-HPCs-N were dispersed in isopropyl alcohol via ultrasound treatment for 30 min and then mixed with a 5 wt% Nafion solution. The mixture was then ultrasonicated for another 30 min and sprayed onto a carbon cloth. 40 wt% Pt-loaded Pt-CB catalysts (Johnson Matthey, USA) were also prepared using a similar method. For the membrane electrode assembly (MEA), the 40 wt% Pt-loaded Pt-CB catalysts were used as the anode catalysts. The electrodes had a geometric area of 4 cm^2 with a Pt loading of 0.2 mg/cm^2. The Pt-HPCs-N and Pt-CB cathodes had geometric areas of 4 cm^2 with a Pt loading of 0.2 mg/cm^2. The MEA was prepared via hot pressing pretreated Nafion 212 (DuPont, USA) sandwiched between the anode and cathode.

2.3. Characterization

The morphologies of the HPCs-N and Pt-HPCs-N were observed using transmission electron microscopy (TEM; JEM2100F, JEOL,

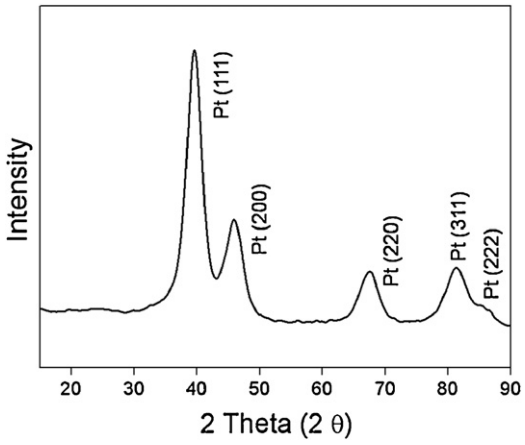

Fig. 2. X-ray diffraction pattern of Pt-HPC-N. Mean Pt particle size was estimated to be 2.2 nm from the Pt (2 2 0) peak.

Japan). Elemental analyses were performed using an EA1112 analyzer (CE Instruments, Italy). The porous properties of the HPCs-N and Pt-HPCs-N were examined using nitrogen adsorption and desorption isotherms that were obtained at −196 °C using the surface area and a porosimetry analyzer (ASAP 2020, Micromeritics, USA). X-ray photoelectron spectroscopy (XPS; PHI 5700 ESCA, Korea) was performed using monochromated Al Kα radiation ($h\nu$ = 1486.6 eV). The Pt loading in the samples was determined using inductively coupled plasma-optical emission spectroscopy (ICP-OES). In order to estimate the electrochemical surface areas (ESAs) of Pt in the carbon-supported Pt catalysts, a three-electrode electrochemical cell was employed, and cyclic voltammetry measurements were taken at room temperature with scan rates of 100 mV/s over the potential range of −0.2 to 1.2 V (vs. Ag/AgCl). The polarization performance tests were conducted at 70 °C using a fuel cell test station. H_2 and O_2 were supplied to the anode and cathode at flow rates of 200 and 600 mL/min, respectively.

3. Results and discussion

The HPCs-N had a 3D interconnected porous structure over a large area, and well-developed open macropores, which were hundreds of nanometers in diameter (Fig. 1a and b). The open macroporous structure remained the same after the Pt nanoparticles were incorporated on the surface (Fig. 1c). In addition, the considerably homogeneous Pt nanoparticles were well-dispered on the carbon surface despite a large amount of 40 wt% Pt nanoparticles (Fig. 1d). The histogram of the Pt nanoparticles obtained from the measurements of over 100 Pt nanoparticles demonstrates that the Pt nanoparticle size was mostly in the range of 2–3 nm (Fig. 1e). This small diameter and high dispersion of Pt nanoparticles were attributed to nitrogen sites that provided the main initial nucleation sites for Pt nanoparticle formation [22]. In addition, the

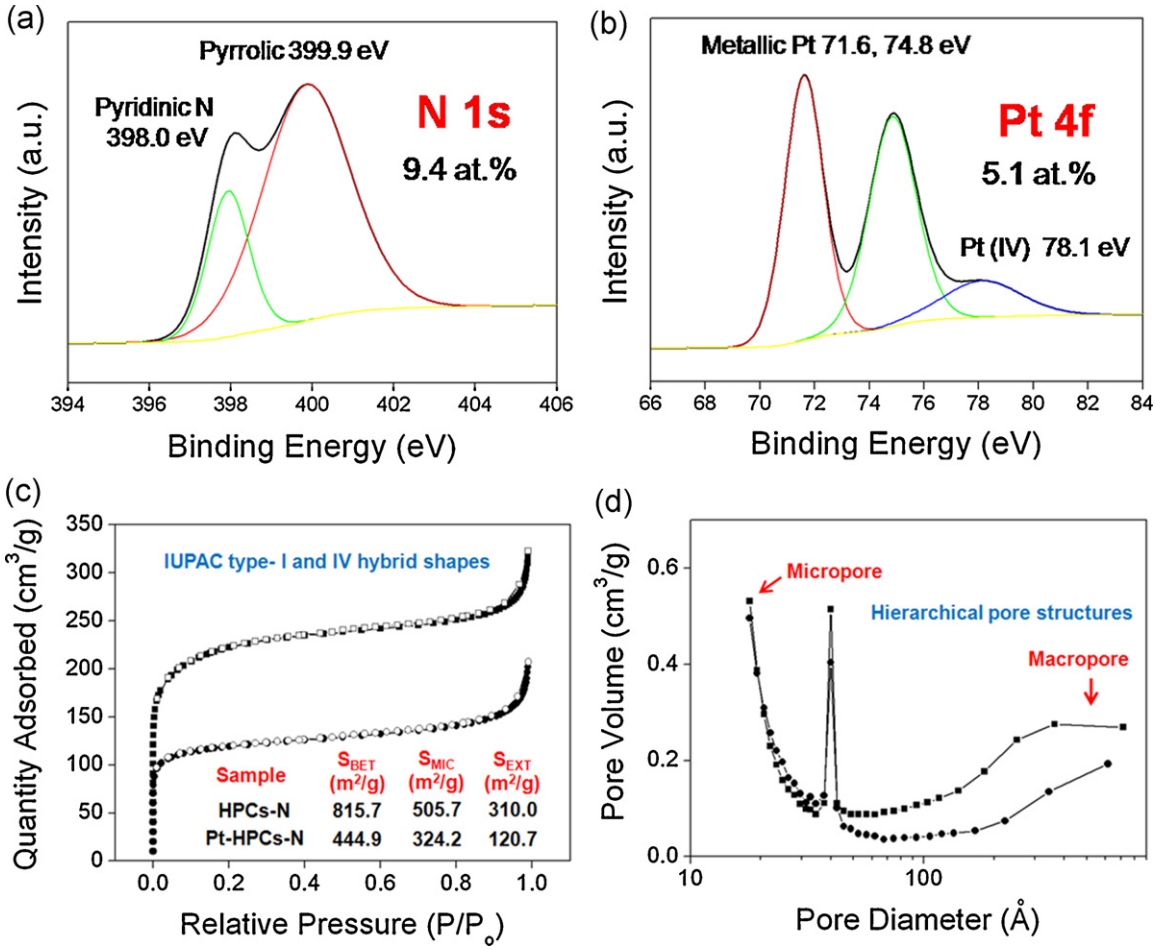

Fig. 3. XPS (a) N 1s spectra and (b) Pt 4f spectra of the Pt-HPCs-N. (c) Nitrogen adsorption and desorption isotherm and (d) pore size distribution of the HPCs-N (cubic) and Pt-HPCs-N (circle).

introduction of nitrogen atoms endows the carbons with a polar nature, which allows easy wetting [23,24]. The mean Pt nanoparticle size was also calculated from XRD patterns, by estimating from the isolated Pt (2 2 0) peak using the Scherrer equation (Fig. 2):

$$L = \frac{0.9\lambda_{K\alpha 1}}{B_{(2\theta)} \cos\theta_{max}} \quad (1)$$

where $\lambda_{K\alpha 1}$ is the X-ray wavelength, θ_{max} is the maximum angle of the (2 2 0) peak, and $B_{(2\theta)}$ is the half-peak width for Pt (2 2 0) in radians. The size of Pt nanoparticles was 2.2 nm, which was consistent with the typical TEM images of the Pt-HPCs-N samples.

The chemical nature and stoichiometry of the nitrogen atoms and Pt nanoparticles were confirmed via XPS measurements (Fig. 3a and b). The compositional analyses indicate approximately 9.4 at.% of nitrogen atoms and 5.1 at.% Pt nanoparticles in the surface region of the samples. The elemental analysis and ICP-OES also indicated the presence of nitrogen atoms and Pt nanoparticles in the Pt-HPCs-N. 6.1 wt% nitrogen atoms and approximately 40 wt% Pt nanoparticles were incorporated in the Pt-HPCs-N. The chemical atmosphere of the nitrogen atoms in the Pt-HPCs-N was primarily in the form of pyrrolic groups and pyridinic nitrogen species, as indicated by the N 1s peaks centered at 399.9 and 398.0 eV, respectively (Fig. 3a). The Pt 4f spectra exhibited an intense doublet (71.6 and 74.8 eV), which is attributed to the metallic Pt (Fig. 3b) [25]. The weak peak at 78.1 eV was most likely caused by a small amount of Pt (IV) species on the surface [25].

The pore characteristics were investigated using nitrogen adsorption and desorption isotherms (Fig. 3c and d). The nitrogen adsorption and desorption isotherms of the HPCs-N and Pt-HPCs-N depict IUPAC type I and IV hybrid shapes, which suggest dual microporous and mesoporous structures (Fig. 3c). The surface area of the HPCs-N was 815.7 m^2/g. The surface area decreased to 444.9 m^2/g after the Pt nanoparticles were incorporated on the surface of the HPCs-N. However, the Pt-HPCs-N had high surface area, and its hierarchical pore structure remained after the Pt nanoparticles were incorporated on the surface of the HPCs-N (Fig. 3d). The high surface area from the mesopores and micropores and the open macroporous structure facilitate simultaneous access between the Pt electrocatalyst, reactant, and Nafion. In addition, the high surface area resulting from the mesopores and micropores can also contribute ORR electrocatalytic activity by providing numerous nitrogen-doped sites. The extension of the three-phase boundary results in the enhancement of the ORR electrocatalytic activity. Fig. 4a shows the cyclic voltammograms of the Pt-HPCs-N and Pt-CB cathodes at a scan rate of 100 mV/s over a potential range of −0.2 to 1.4 V. The ESAs of the Pt in the supported Pt (40 wt%) catalysts were determined from the integrated charge in the hydrogen adsorption region of the steady-state cyclic voltammograms in the supporting electrolyte. The ESA was calculated as 55.2 m^2/g for the Pt in the Pt-HPCs-N cathode, which is significantly larger than the 36.5 m^2/g measured for the Pt in the Pt-CB cathode, indicating higher utilization of the Pt-HPCs-N induced by the open macroporous structure and nitrogen atoms. The improvement in H adsorption is related to the ease of access to the Pt nanoparticles because of the open macropores. The ORR electrocatalytic activities of the Pt-HPCs-N and Pt-CB cathodes were evaluated using Nyquist plots, as shown in Fig. 4b. The semicircular diameter of the Pt-HPCs-N cathode was much smaller than that of the Pt-CB cathode. This suggests that the ORR charge transfer resistance was much smaller at the Pt-HPCs-N cathode catalysts. Fig. 5 shows the polarization curves of the Pt-HPCs-N and Pt-CB cathodes. In the region of very low current density, a rapid voltage drop in the potential–current curve, which is generally known as an activation polarization, reflects the sluggish kinetics intrinsic to the ORR at the cathode surface. The voltage drop of the Pt-HPCs-N cathode was smaller than that of the Pt-CB cathode. This indicates

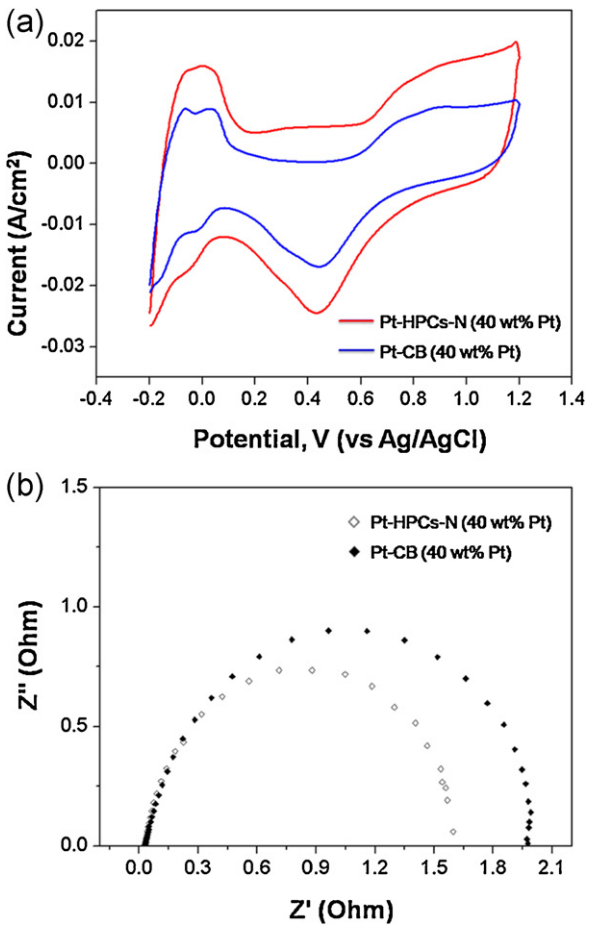

Fig. 4. (a) Cyclic voltammograms of the Pt-HPCs-N cathode at a scan rate of 100 mV/s over a potential range of −0.2 to 1.2 V (0.2 mg Pt/cm^2) and (b) Nyquist plots for the Pt-HPCs-N cathode (0.2 mg Pt/cm^2), a frequency range from 2000 Hz to 0.05 Hz with an amplitude of 1 mA at 70 °C in OCV condition.

better kinetics in the ORR of the Pt-HPCs-N cathode. The improved performance can be attributed to the improved carbon-catalyst binding and open macroporous structure with a relatively high three-phase boundary. It can also be considered as a synergistic support effect with the HPCs-N, because the nitrogen-doped carbon nanostructures are known to decompose reactive intermediates such as hydrogen peroxide into oxygen during the ORR [16]. The

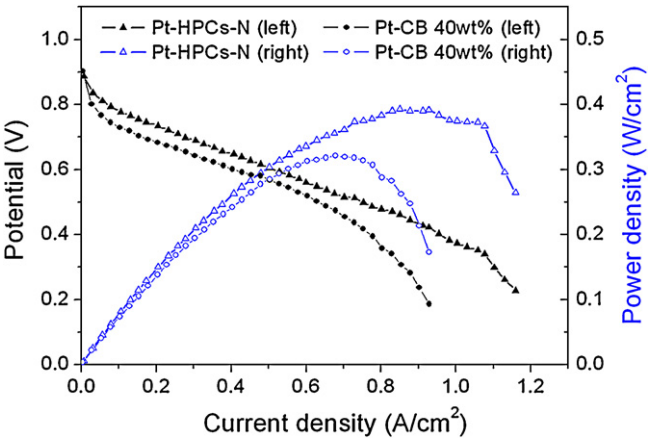

Fig. 5. Polarization and power density plots at 70 °C of the single MEA using Pt-HPCs-N and Pt-CB cathodes (0.2 mg Pt/cm^2), respectively.

Pt-HPCs-N cathode exhibited a mass transfer limitation in a higher current density region than the Pt-CB cathode. The open macroporous structure in the Pt-HPCs-N cathode provides a fast pathway to the active sites through which the reactant and products can be transported readily from the active sites, and by which they can avoid the mass transport limitation. Therefore, the performance of the Pt-HPCs-N cathode was much higher than that of the Pt-CB cathode. The maximum power densities for the Pt-HPCs-N and Pt-CB cathodes were 393 mW/cm^2 and 322 mW/cm^2, respectively. The value of the maximum power densities for the Pt-HPCs-N was about 2 kW/g Pt, which is much higher than the values (1.1 kW/g Pt and 0.88 kW/g Pt) for the nitrogen-doped multi-walled carbon nanocoils and nitrogen-doped graphene nanoplatelets [17,18]. As a result, the performance of a single MEA was increased by 22% using the Pt-HPCs cathode, indicating better efficiency of the Pt catalysts through the use of a novel nanostructured catalyst support.

4. Conclusion

A cathode with homogeneous small diameter and high dispersion of Pt catalysts was prepared using a novel carbon as a catalyst support. The ESA of Pt in the Pt-HPCs-N cathode (55.2 m^2/g) was much higher than that of the Pt in the Pt-CB cathode (36.5 m^2/g). The ORR charge transfer resistance was also much smaller for the Pt-HPCs-N cathode catalysts. The full cell performance of a single MEA using a Pt-HPCs-N cathode (393 mW/cm^2) was 22% higher than that of a single MEA using a Pt-CB cathode (322 mW/cm^2).

Acknowledgement

This work was supported by the National Research Foundation of Korea Grant funded by the Korean Government (MEST) (NRF-2010-C1AAA001-0029018).

References

[1] R.F. Service, Science 296 (2002) 1222–1224.
[2] S. Srinivasan, R. Mosdale, P. Stevens, C. Yang, Annual Review of Energy and the Environment (1999) p281.
[3] Y. Shao, J. Liu, Y. Wang, Y. Lin, Journal of Materials Chemistry 19 (2009) 46–59.
[4] S.H. Joo, S.J. Choi, I. Oh, J. Kwak, Z. Liu, O. Terasaki, R. Ryoo, Nature 412 (2001) 169–172.
[5] H. Chang, S.H. Joo, C. Pak, Journal of Materials Chemistry 17 (2007) 3078–3088.
[6] J.-S. Yu, S. Kang, S.B. Yoon, G. Chai, Journal of the American Chemical Society 124 (2002) 9382–9383.
[7] B. Fang, J.H. Kim, M. Kim, J.-S. Yu, Chemistry of Materials 21 (2009) 789–796.
[8] L. Calvillo, M. Gangeri, S. Perathoner, G. Centi, R. Moliner, M.J. Lazaro, International Journal of Hydrogen Energy 36 (2011) 9805–9814.
[9] M.M. Bruno, E.A. Franceschini, F.A. Viva, Y.R.J. Thomas, H.R. Corti, International Journal of Hydrogen Energy, http://dx.doi.org/10.1016/j.ijhydene.2012.02.058
[10] R. Balgis, G.M. Anilkumar, S. Sago, T. Ogi, K. Okuyama, Journal of Power Sources 203 (2012) 26–33.
[11] S. Kundu, T.C. Nagaiah, X. Chen, W. Xia, M. Bron, W. Schuhmann, M. Muhler, Carbon 50 (2012) 4534–4542.
[12] Y.S. Yun, H. Bak, H.-J. Jin, Synthetic Metals 160 (2010) 561–565.
[13] Y.S. Yun, D. Kim, Y. Tak, H.-J. Jin, Synthetic Metals 161 (2011) 2460–2465.
[14] Y. Shao, J. Sui, G. Yin, Y. Gao, Applied Catalysis B: Environmental 79 (2008) 89–99.
[15] S.-H. Liu, J.-R. Wu, International Journal of Hydrogen Energy 36 (2011) 87–93.
[16] S. Maldonado, K.J. Stevenson, Journal of Physical Chemistry B 109 (2005) 4707–4716.
[17] R. Imran Jafri, N. Rajalakshmi, S. Ramaprabhu, Journal of Power Sources 195 (2010) 8080–8083.
[18] R. Imran Jafri, N. Rajalakshmi, S. Ramaprabhu, Journal of Materials Chemistry 20 (2010) 7114–7117.
[19] Y. Chen, J. Wang, H. Liu, M.N. Banis, R. Li, X. Sun, T.-K. Sham, S. Ye, S. Knights, Journal of Physical Chemistry C 115 (2011) 3769–3776.
[20] X. Tuaev, J.P. Paraknowitsch, R. Illgen, A. Thomas, P. Strasser, Physical Chemistry Chemical Physics 14 (2012) 6444–6447.
[21] Y.S. Yun, J. Shim, Y. Tak, H.-J. Jin, RSC Advances 2 (2012) 4353–4358.
[22] C.-L. Sun, L.-C. Chen, M.-C. Su, L.-S. Hong, O. Chyan, C.-Y. Hsu, K.-H. Chen, T.-F. Chang, L. Chang, Chemistry of Materials 17 (2005) 3749–3753.
[23] K. Jiang, A. Eitan, L.S. Schadler, P.M. Ajayan, R.W. Siegel, Nano Letters 3 (2003) 275–277.
[24] M. Endo, Y.A. Kim, M. Ezaka, K. Osada, T. Yanagisawa, T. Hayashi, M. Terrones, M.S. Dresselhaus, Nano Letters 3 (2003) 723–726.
[25] Z. Liu, L.M. Gan, L. Hong, W. Chen, J.Y. Lee, Journal of Power Sources 139 (2005) 73–78.